PAPER

Check for updates

Methyl itaconate–anthracene adducts (MIAs) facilitate the enantiomeric separation of 1,1′-bi-2-naphthols *via* thin-layer chromatography (TLC) with trends predicted by molecular dynamics simulations

Wichai Sinthopweha,[ab] Nopawit Khamto,[c] Puracheth Rithchumpon[d] and Puttinan Meepowpan [ID] *[aef]

1,1′-bi-2-naphthols (BINOLs) and their derivatives have been extensively studied over the years. Enantiopure BINOLs are crucial in asymmetric synthesis, circularly polarized luminescent dyes, and charge transfer host systems. Several methods, including asymmetric oxidative coupling, enzymatic resolution, and chemical resolution, have been explored to prepare enantiopure BINOLs. Chemical resolution by chromatography offers the advantage of obtaining both enantiomers with high purity. Herein, we employed methyl itaconate–anthracene adducts (MIAs) as chiral resolving agents (CRAs) for the resolution of racemic BINOLs. Diastereomers were obtained *via* esterification in yields ranging from 37% to 62%. ^{1}H NMR revealed distinct H_y proton behaviors, correlating with the orientation of the second naphthol ring as predicted by DFT calculations. In the diastereomers without 3,3′-dibromo-substituted BINOLs, the H_y protons were shielded from the anisotropic effect, whereas 3,3′-dibromo-substituted BINOLs diastereomers exhibited the opposite effect. MIAs effectively resolved racemic BINOLs on TLC, showing significant differences in retardation factor (R_f). Molecular dynamics simulations predicted TLC resolution trends by examining the number of hydrogen bonds between diastereomers and silica gel. For diastereomers without 3,3′-dibromo-substituted BINOLs, the (S,S)-diastereomers formed more hydrogen bonds than the (S,R)-diastereomers, resulting in lower R_f values. Conversely, for diastereomers of 3,3′-dibromo-substituted BINOLs, the (S,R)-diastereomers exhibited stronger hydrogen bonding.

Introduction

1,1′-bi-2-naphthols (BINOLs) and their derivatives are axially chiral compounds, characterized by a mode of stereoisomerism in which a central axis restricts rotation around a single bond, resulting in a nonplanar arrangement of four substituents in specific pairs.[1] BINOLs have been extensively explored for various applications over a long period. Notably, enantiopure BINOL forms significantly influence the configuration and purity of

enantioselective products,[2,3] especially in asymmetric synthesis. Their applications in this field are broad, encompassing reductions, oxidations, aldol reactions, Mannich reactions, and Diels–Alder reactions.[4,5] Beyond synthesis, enantiopure BINOLs have also been investigated in diverse areas such as circularly polarized luminescence (CPL) dyes,[6] charge transfer host systems,[7] and supramolecular chemistry.[8]

Due to the importance of enantiopure BINOLs, several methods have been developed for their preparation. Currently, three contemporary strategies have emerged for the resolution of chiral mixtures: asymmetric synthesis *via* the oxidative coupling of 2-naphthol, enzymatic resolution, and chemical chiral resolution utilizing either crystallization or chromatographic techniques.[9,10] Among these, chemical chiral resolution has proven particularly efficient, offering good yields with high enantioselectivity. Chromatographic techniques, in particular, offer distinct advantages over crystallization, as they do not require crystalline materials and can produce both enantiomers of BINOLs in optically pure forms.[11] While column liquid and gas chromatography are commonly used for chiral resolution, thin-layer chromatography (TLC) stands out as the most accessible method for both directly

[a] Department of Chemistry, Faculty of Science, Chiang Mai University, 239 Huay Kaew Road, Chiang Mai 50200, Thailand. E-mail: puttinan.m@cmu.ac.th

[b] Multidisciplinary and Interdisciplinary School, Chiang Mai University, 239 Huay Kaew Road, Chiang Mai 50200, Thailand

[c] Department of Biochemistry, Faculty of Medical Science, Naresuan University, Phitsanulok 65000, Thailand

[d] Department of Chemistry, Faculty of Science, Khon Kaen University, Khon Kaen 40002, Thailand

[e] Center of Excellence for Innovation in Chemistry (PERCH-CIC), Chiang Mai University, 239 Huay Kaew Road, Chiang Mai 50200, Thailand

[f] Center of Excellence in Materials Science and Technology, Chiang Mai University, 239 Huay Kaew Road, Chiang Mai 50200, Thailand

resolving racemates and monitoring enantiomeric purity, primarily due to its simplicity, flexibility, and low cost.[12]

Chiral resolving agents (CRAs) are essential in chromatographic resolution, as they facilitate the separation of enantiomers by forming diastereomers with distinct physical properties.[13] Numerous CRAs, as depicted in Fig. 1, have been investigated for the resolution of racemic BINOLs.[11,14–18]

However, the preparation of these CRAs in pure form remains challenging. Furthermore, the specific interactions that govern the differential adsorption capacities during the TLC resolution process have not yet been fully elucidated.

Methyl itaconate–anthracene adducts (MIAs) are chiral compounds that can be readily synthesized in high overall yields through conventional reactions. MIAs and structurally related analogues have previously been reported as chiral derivatizing agents (CDAs) for determining the absolute configuration of

chiral secondary alcohols and primary amines.[19–21] In these applications, the distinct structures of the resulting diastereomers lead to different chemical shifts for specific protons in their ^1H NMR spectra, which enables the assignment of absolute configuration. In this study, we employed MIAs as CRAs for the resolution of racemic BINOLs and their derivatives, as depicted in Fig. 1. Moreover, we predicted the proton chemical shifts of the diastereomers using density functional theory (DFT) calculations. Additionally, on TLC, their absolute configurations were preliminarily studied, and the interaction between each diastereomer and silica gel was elucidated using molecular dynamics (MD) simulations. The BINOL derivatives and BINAMs which applied in this study were exhibited in Fig. 2.
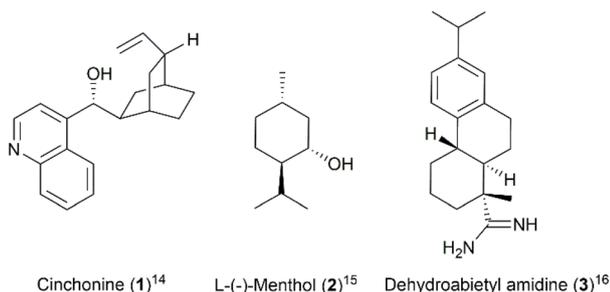
Results and discussion

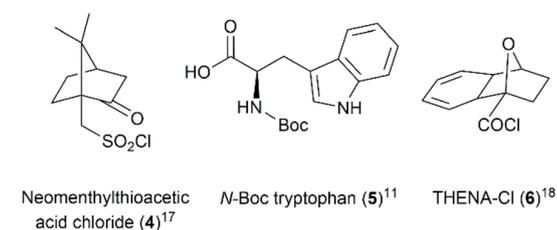### Enantiopure synthesis of (11S)-MIA and (11R)-MIA (7 and 8)

Enantiopure (11S)-7 and (11R)-8 were synthesized through a Diels–Alder reaction between dimethyl itaconate and anthracene. The resulting product then underwent hydrolysis, followed by esterification with (–)-menthol for chiral resolution, and finally transmethylation to yield both enantiopure dimethyl itaconate–anthracene adducts.[19] Each of these enantiomers was subsequently subjected to complete hydrolysis and selective methylation, following the procedures outlined in references,[20,21] to produce the final enantiopure (11S)-7 and (11R)-8. In these studies, the enantiomeric purity (11S)-(7) was chosen to preliminarily determine its ability to resolve the racemic BINOL derivatives.
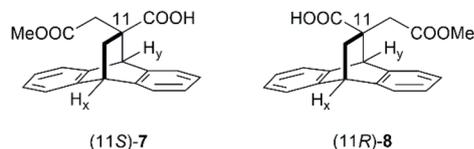
Fig. 1 (Top) Lists of CRAs for BINOLs resolution by crystallization and chromatography, (Bottom) application of MIAs and their key advantages.
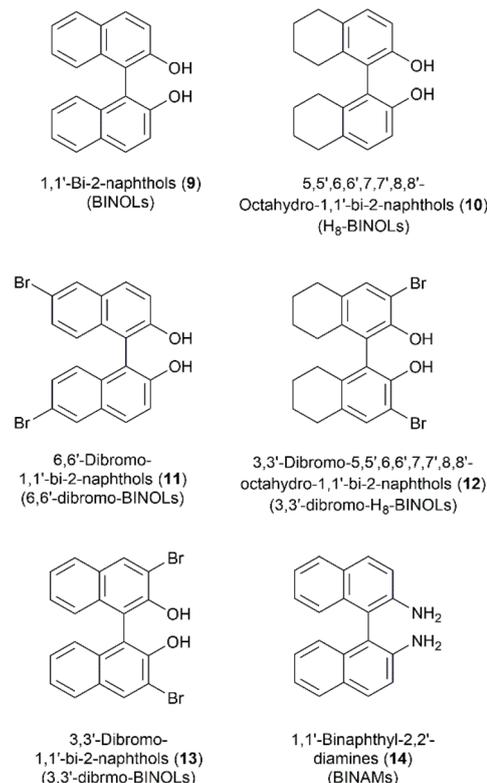

Fig. 2 Chemical structures of BINOL derivatives and BINAMs which were applied in this research.

Synthesis of diastereomers of (11S)-MIA-BINOL derivatives

Diastereomers **15a–d** and **16a–d** were synthesized through an esterification reaction under mild conditions, using N,N'-dicyclohexylcarbodiimide (DCC) and 4-dimethylaminopyridine (DMAP). The crude product was filtered to remove dicyclohexylurea and further purified using chromatographic technique to afford the desired diastereomers in 37% to 62% yields (Scheme 1).

However, diastereomers formed between (11S)-**7** and 3,3′-dibromo-BINOLs, as well as BINAMs, could not be synthesized using these conditions due to the steric hindrance effect. To overcome this limitation, (11S)-**7** was first treated with oxalyl chloride and triethylamine at room temperature for 4 h. The resulting crude adduct was evaporated to dryness under vacuum without further purification. Subsequently, either 3,3′-dibromo-BINOLs or BINAMs was added to the crude adduct along with a few drops of triethylamine. The mixture was stirred for 24 h, yielding diastereomers **15e–f** and **16e–f** in 41% to 44% yields (Scheme 2).

^{1}H NMR characteristics of each diastereomer

The ^{1}H NMR analysis of (11S)-MIA-BINOL derivatives in CDCl$_3$ revealed significant differences in chemical shifts between each diastereomer, especially for the H$_y$ proton of (11S)-**7**. For pairs without 3,3′-dibromo-substituted BINOLs (**15a–c** and **16a–c**), the H$_y$ protons were shielded by the naphthalene moiety's anisotropic effect.

Notably, the H$_y$ proton of the (S,R)-diastereomers **15a–c** was more shielded than that of the (S,S)-diastereomers **16a–c** (Fig. 3 and S1). However, in diastereomers containing 3,3′-dibromo-substituted BINOLs (**15d–e** and **16d–e**), the H$_y$ protons exhibited a deshielding effect, a pattern not observed previously (Fig. 4 and S2). It is also worth noting that the behavior of BINAM diastereomers (**15f** and **16f**), which are amide compounds, differed from that of BINOL ester diastereomers. While the chemical shifts of their H$_y$ protons remained unchanged between these amide diastereomers, the H$_x$ protons showed a significant shift (Fig. 5 and S3). The difference of chemical shift values of H$_x$ and H$_y$ of each derived adduct was compared and displayed in Table 1.

Investigating the behaviour of diastereotopic H$_y$ protons in ^{1}H NMR spectra using computational simulation

The distinct behaviours of the H$_y$ proton in the ^{1}H NMR spectra were investigated and elucidated through DFT calculations. Conformations were effectively sampled using the Low-ModeMD,[22] a superior approach that perturbs an existing system along with molecular dynamics simulations. All conformations were primarily optimized for their more stable
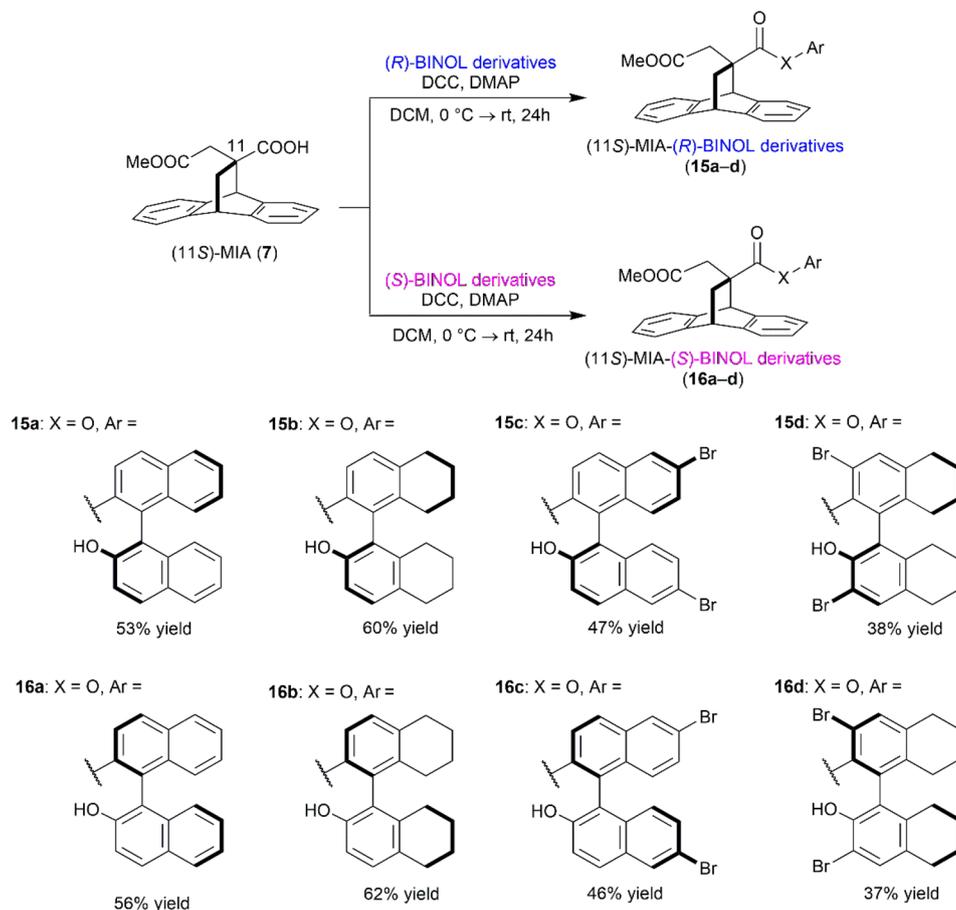
Scheme 1 Synthesis of diastereomers **15a–d** and **16a–d** using DCC and DMAP as coupling reagent.
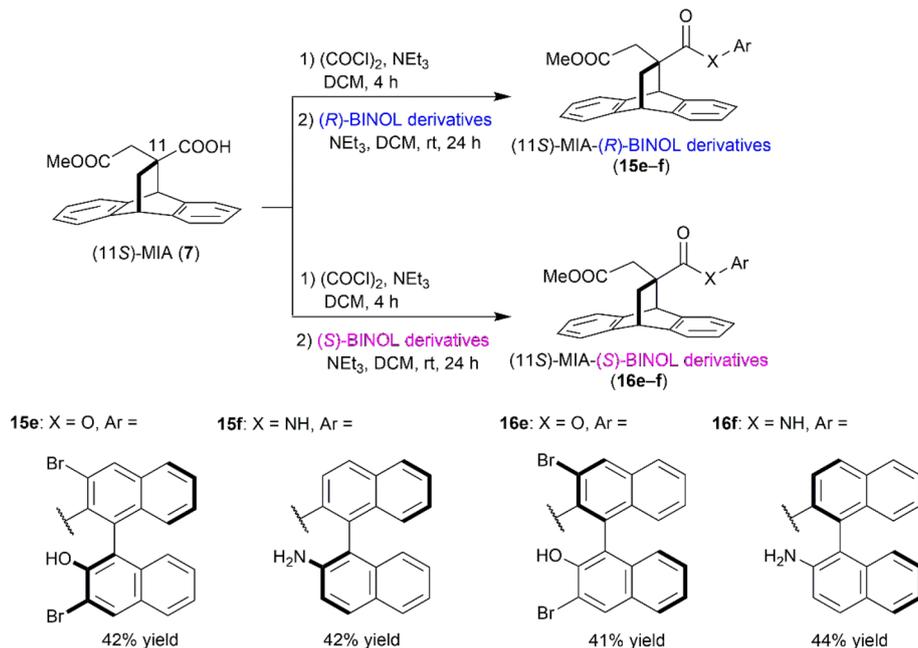
Scheme 2 Synthesis of diastereomers **15e–f** and **16e–f** using (COCl)$_2$ as coupling agent.

conformer based on DFT/B3LYP 6-31G (d,p) level of theory. X-ray crystallography experiments depicted in Fig. 6, however, indicated the presence of dispersion forces, such as π–π and π–σ interactions between aromatic rings. So, we used *meta*-GGA functional M06-2X with 6-311++G (d,p) basis set to specifically study these interactions. To benchmark our approach, the root-mean-square deviation (RMSD) of the superimposition between

the calculated and native (X-ray) structures was 1.22 Å, Fig. S53, indicating excellent correlation with the experimental data.

Diastereomers without 3,3′-dibromo-substituted BINOLs (**15a–c**, **16a**, and **16c**) exhibited π–σ interactions between the H$_y$ proton and the second naphthol ring (the one not forming a bond), with the exception of **16b**. Additionally, π–π T-shaped interactions between the anthracene and the second naphthol ring further stabilized these diastereomers. In contrast, diastereomers with
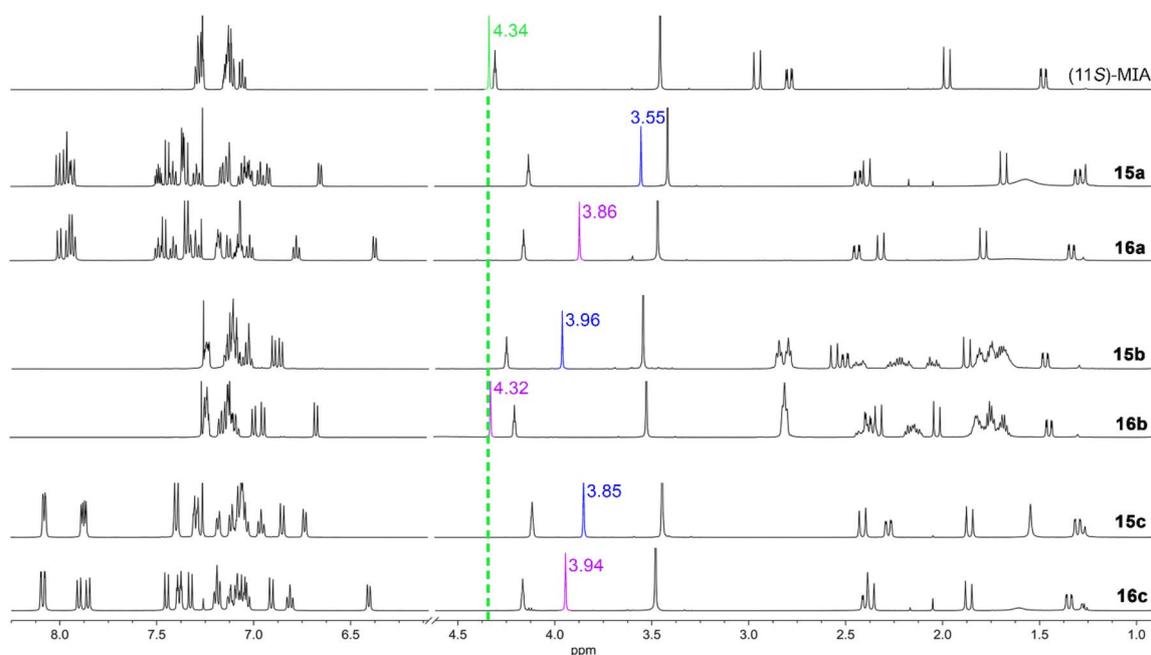
Fig. 3 Comparison of ^{1}H NMR (500 MHz, CDCl$_3$) spectra of each diastereomer of BINOLs (**15a** and **16a**), H$_8$-BINOLs (**15b** and **16b**), and 6,6′-dibromo-BINOLs (**15c** and **16c**), with colour higlighted for H$_y$ proton; blue represents the (*S,R*)-diastereomers; purple represents the (*S,S*)-diastereomers.
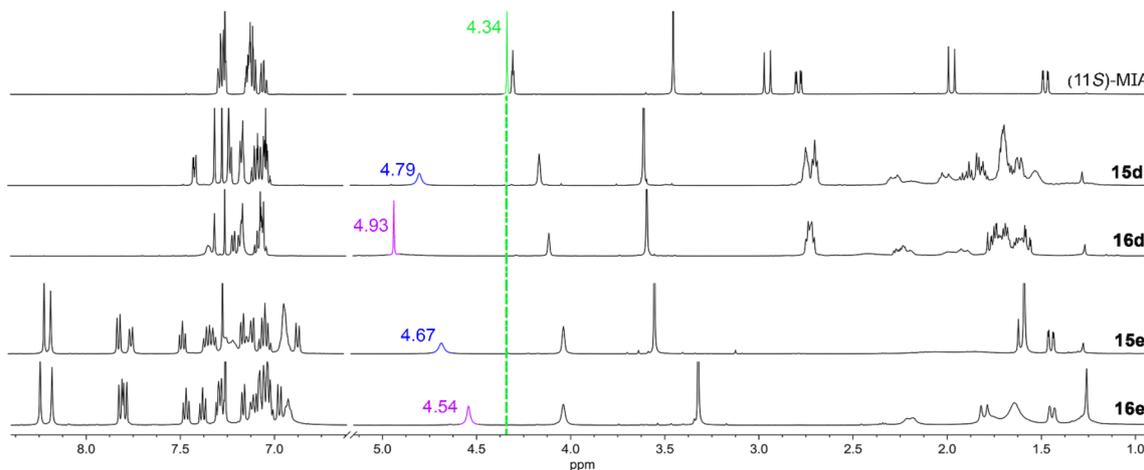
Fig. 4 Comparison of ^{1}H NMR (500 MHz, CDCl$_3$) spectra of each diastereomers of 3,3′-dibromo-H$_8$-BINOLs (**15d** and **16d**) and 3,3′-dibromo-BINOLs (**15e** and **16e**), with colour higlighted for H$_y$ proton; blue represents the (S,R)-diastereomers; purple represents the (S,S)-diastereomers.

3,3′-dibromo-substituted BINOLs (**15d–e** and **16d–e**) behaved differently. The large bromine atoms at the 3 and 3′ positions of BINOLs created strong repulsion between the bromine on the first naphthol ring (the bonded ring) and the carbonyl oxygen (C=O···3p), as shown in Table 2. As a result, the second naphthol ring aligned away from the H$_y$ proton and the anthracene, eliminating any interactions (Fig. 7). Based on previous results, π–σ interaction caused a shielding anisotropic effect, leading to a lower chemical shift, while the absence of π–σ interaction resulted in a deshielding anisotropic effect. Notably, the C=O···3p distances in the (S,R)-diastereomers **15a–f** were consistently greater than those in the (S,S)-diastereomers **16a–f**. In the case of BINAM diastereomers **15f** and **16f**, the H$_y$ protons' behaviour was entirely different from the BINOL ester compounds. This is primarily due to the persistent hydrogen atom of the N–H amide bond. This hydrogen atom interacted with the anthracene through π-donor hydrogen bonding, causing the second naphthol ring to rotate away from the (11S)-**7**, which did not significantly affect the H$_y$ proton.

Validation of efficacy of MIA as chiral resolving agents of (rac)-BINOL derivatives

To achieve the optimal resolution of each diastereomer, we tested various mobile phase systems as eluents. The optimal eluent and its ratio were identified, enabling the separation of each diastereomers with distinct R_f differences (ΔR_f) ranging from 0.08 to 0.15 (Table 3). In addition, we observed different patterns in the TLC resolution that were consistent with the trends found in ^{1}H NMR. Specifically, for diastereomers without 3,3′-dibromo-substituted BINOLs (**15a–c** and **16a–c**), the (S,R)-diastereomers **15a–c** had higher R_f values than the (S,S)-diastereomers **16a–c** (Fig. 8a–c). In contrast, for diastereomers containing 3,3′-dibromo-substituted BINOLs (**15d–e** and **16d–e**), and BINAM (**15f** and **16f**), the (S,S)-diastereomers **16d–f** showed higher R_f values compared to the (S,R)-diastereomers **15d–f** (Fig. 8d–f).

A parallel experiment with (11R)-**8** revealed results that were opposite to those observed with (11S)-**7** in both ^{1}H NMR characterization and TLC resolution. Although the H$_y$ protons of diastereomers without 3,3′-dibromo-substituted BINOLs were shielded, the (R,S)-diastereomers displayed greater shielding than the (R,R)-diastereomers. Similarly, when considering diastereomers containing 3,3′-dibromo-substituted BINOLs, the H$_y$ protons remained deshielded, but their chemical shifts were notably reversed (Table S1). Regarding TLC resolution, using the same eluents and ratios, the (R,S)-diastereomers consistently exhibited higher R_f values for diastereomers without 3,3′-dibromo-substituted BINOLs. Conversely, the (R,R)-

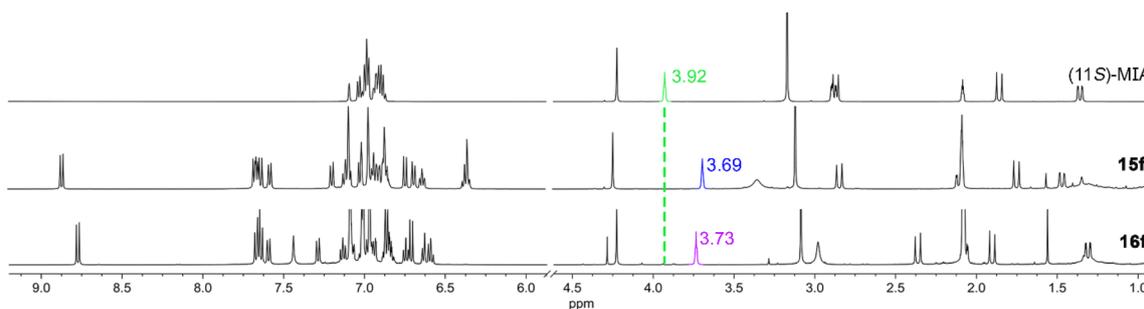

Fig. 5 Comparison of ^{1}H NMR (500 MHz, toluene-d_8) spectra of each diastereomer of BINAMs (**15f** and **16f**), with colour higlighted for H$_y$ proton; blue represents the (S,R)-diastereomer; purple represents the (S,S)-diastereomer.

Table 1 Comparison of H_x and H_y proton chemical shifts in each diastereomers of (11S)–MIA–BINOL derivatives (500 MHz, CDCl$_3$) with (11S)–(**7**)

		Chemical shift (δ, ppm)			
		H_x		H_y	
Entry	BINOL derivatives and BINAMs	(S,R)-**15**	(S,S)-**16**	(S,R)-**15**	(S,S)-**16**
1	BINOLs (**9**)	4.13	4.15	3.55	3.86
2	H$_8$-BINOLs (**10**)	4.25	4.20	3.96	4.32
3	6,6′-Dibromo-BINOLs (**11**)	4.11	4.17	3.85	3.94
4	3,3′-Dibromo-H$_8$-BINOLs (**12**)	4.15	4.11	4.79	4.93
5	3,3′-Dibromo-BINOLs (**13**)	4.02	4.04	4.67	4.54
6	BINAMs (**14**)	3.69[a]	3.73[a]	4.24[a]	4.23[a]
7	(11S)-(**7**)	4.30		4.34	
		3.92[a]		4.18[a]	

[a] in toluene-d_8.

diastereomers showed higher R_f values for diastereomers containing 3,3′-dibromo-substituted BINOLs and BINAMs (Table S2).

Unbiased molecular dynamics simulations were conducted to investigate the atomic-level interactions between the compounds and the silica gel surface. Three independent 100 ns simulations were performed using representative diastereomers: **15a** and **16a** (without 3,3′-dibromo-substituted BINOLs), **15e** and **16e** (containing 3,3′-dibromo-substituted BINOLs), and **15f** and **16f** (BINAMs). The distance and number of hydrogen bonds formed between each compound and the silica gel surface were measured (Fig. S55). Our results indicate that all compounds absorbed onto the silica gel surface during the simulation timescale. The binding poses illustrating these interactions are presented in Fig. 9.

The number of hydrogen bonds demonstrated a strong correlation with the R_f values. Diastereomers with a lower number of hydrogen bonds exhibited higher R_f values. For (11S)-MIA-BINOLs, the (S,R)-diastereomer **15a** formed an average of 0.64 ± 0.44 hydrogen bonds, which was lower than the (S,S)-diastereomer **16a**, with 1.32 ± 0.26 bonds. The (S,S)-diastereomer aligned its OH group to interact with the silanol group of silica gel, resulting in stronger hydrogen bonding, while the OH group of the (S,R)-diastereomer aligned outward (Fig. 9a). The trends observed in TLC were similar for other BINOL derivatives without 3,3′-dibromo-substituted BINOLs,

specifically (11S)-MIA-H$_8$-BINOLs (**15b** and **16b**) and (11S)-MIA-6,6′-dibromo-BINOLs (**15c** and **16c**). This suggests that the aromatic system and the substituents at the C5–C10 positions did not significantly affect interactions with the silica gel surface. In the case of (11S)-MIA-3,3′-dibromo-BINOLs (**15e** and **16e**), the trend was opposite to the previous observations. The binding poses of **15e** and **16e** (Fig. 9b) demonstrated that the presence of bromine atoms at the C-3 and C-3′ positions on BINOLs increased interactions with the silica gel surface, notably *via* hydrogen bonding between the silanol groups and the halogen atoms. This specific interaction was also observed for (11S)-MIA-3,3′-dibromo-H$_8$-BINOLs (**15d** and **16d**), further emphasizing the minimal effect of substituents at C5–C10. For (11S)-MIA-BINAMs, the (S,R)-diastereomer **15f** showed greater hydrogen bonding to silica gel due to the alignment of its amino group (from the BINAM moiety) toward the silica gel surface. Conversely, the (S,S)-diastereomer **16f** positioned its amino group outward, leading to fewer interactions, as only the ester's carbonyl group formed hydrogen bonds with the silica gel (Fig. 9c).

Experimental section

General consideration and materials

All reactions were carried out under nitrogen atmosphere. Unless otherwise noted, materials were obtained from
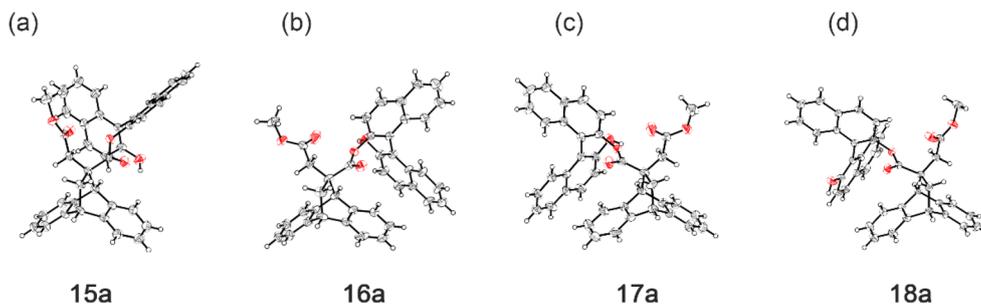

Fig. 6 ORTEP diagram from single crystal-XRD of (a) (11S)–MIA–(R)–BINOL (**15a**), (b) (11S)–MIA–(S)–BINOL (**16a**), (c) (11R)–MIA–(R)–BINOL (**17a**), and (d) (11R)–MIA–(S)–BINOL (**18a**).

Table 2 Interactions between the H_y proton, and part of anthracene, to the second naphthol ring from optimized structures using DFT calculation at M06-2X/6-31++G (d,p) level

| Compound | Interaction | | Atom type at C-3 | Distance of C=O···3p (Å) |
	The H_y proton to second naphthol ring	The anthracene to second naphthol ring		
15a	π–σ	3 (π–π T-shaped)	H	2.635
16a	π–σ	3 (π–π T-shaped)	H	2.221
15b	π–σ	π–π T-shaped	H	2.636
16b	—	π–π T-shaped	H	2.403
15c	π–σ	2 (π–π T-shaped)	H	2.365
16c	π–σ	3 (π–π T-shaped)	H	2.234
15d	—	—	Br	3.636
16d	—	—	Br	3.317
15e	—	—	Br	3.291
16e	—	—	Br	3.192
15f	—	2 (π–π stacked)	H	2.306
16f	—	π–π stacked	H	2.172
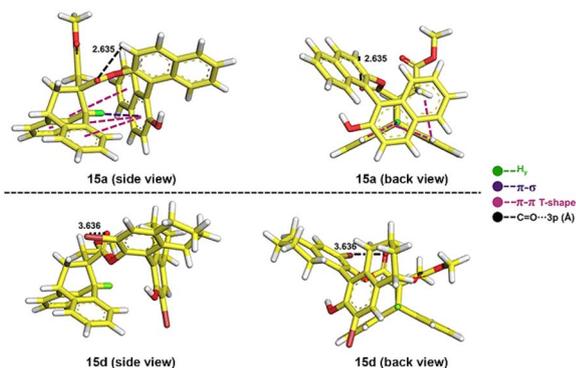
Fig. 7 Interactions exhibited in representative diastereomers **15a** and **15d** at M06-2X/6-31++G (d,p).

(cm^{-1}). The high-resolution mass spectra (HRMS, m/z values) were obtained from Agilent 6540 UHD Quadrupole Time-of-Flight (Q-TOF) mass spectrometer. ^1H and ^{13}C NMR spectra were recorded on a Bruker Neo™ 500 MHz spectrometer. Where necessary, 2D NMR experiments (HMBC and HMQC) were carried out to assist the structure elucidation and signal assignment. The chemical shifts were given in ppm downfield from tetramethylsilane (TMS). All NMR spectra were measured in $CDCl_3$ and toluene-d_8. The chemical shifts were reported as δ-values in parts per million (ppm) relative to the residue $CHCl_3$ as internal reference (^1H: δ 7.26, ^{13}C: δ 77.00) and residual toluene as internal reference (^1H of CH_3: δ 2.08, ^{13}C of CH_3: δ 20.43) and coupling constants (J values) were reported in hertz (Hz). Peak multiplicities are indicated as follows: s (singlet), d (doublet), t (triplets), dt (doublet of triplets), ddd (doublet of doublets of doublets), ddt (doublet of doublets of triplets) and m (multiplets). Flash column chromatography was performed employing Merck silica gel 60 and Merck silica gel 60H. Preparative thin layer chromatography (PLC) plates were carried out using Merck silica gel 60 PF_{254}. Analytical thin layer chromatography was performed with Merck silica gel 60 PF_{254} aluminum plates. All the reactions were conducted on oven-dried glassware, under N_2, with anhydrous solvents, which

commercial suppliers and used without further purification. Melting points were determined by using a Gallenkamp Electrothermal apparatus and were uncorrected. Optical rotations were measured in $CHCl_3$ on a Rudolph Research Analytical Autopol I Automatic Polarimeter. Infrared spectra were recorded on a FT-IR model TENSER 27 (Bruker) spectrometer and absorption frequencies were reported in reciprocal centimeters

Table 3 Application of (11S)-7 for chiral BINOL derivatives resolution using TLC techniques as R_f, along with the average number of hydrogen bonds from MD simulations

| Entry | BINOL derivatives and BINAMs | (S,R)-**15** | | (S,S)-**16** | | ΔR_f |
		R_f	#H-bond[e]	R_f	#H-bond[e]	
1	BINOLs (**9**)	0.69[a]	0.64 ± 0.44	0.58[a]	1.32 ± 0.26	0.11
2	H_8-BINOLs (**10**)	0.44[a]	ND	0.34[a]	ND	0.10
3	6,6′-Dibromo-BINOLs (**11**)	0.57[a]	ND	0.42[a]	ND	0.15
4	3,3′-Dibromo-H_8-BINOLs (**12**)	0.57[b]	ND	0.65[b]	ND	0.08
5	3,3′-Dibromo-BINOLs (**13**)	0.44[c]	1.00 ± 0.37	0.57[c]	0.28 ± 0.20	0.13
6	BINAMs (**14**)	0.31[d]	1.26 ± 0.35	0.42[d]	0.98 ± 0.64	0.11

[a] 20% EtOAc/hexane. [b] 10% EtOAc/hexane. [c] 80% DCM/hexane. [d] 10% EtOAc 40% DCM/hexane. [e] Measured based on unbiased three independent MD simulations.
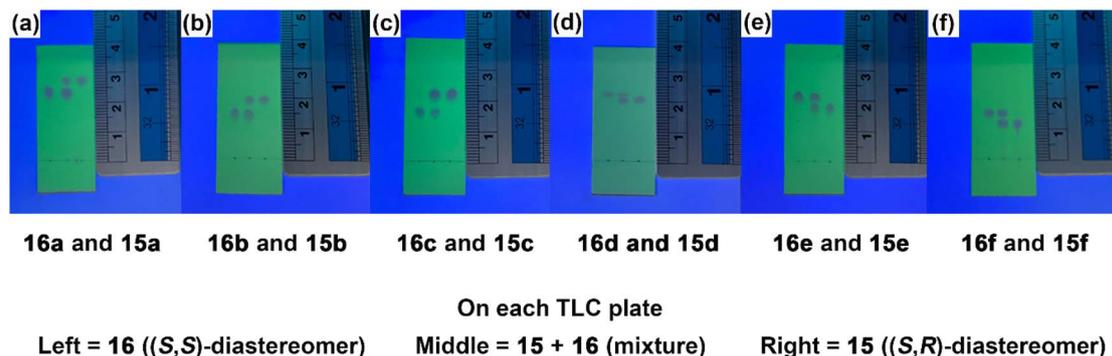
Fig. 8 Investigation of chiral resolution capability of MIA using TLC plates of each diastereomer of (11S)-MIA-BINOL derivatives with eluent systems: (a) (11S)-MIA-BINOLs (15a and 16a) (20% EtOAc/hexane), (b) (11S)-MIA-H$_8$-BINOLs (15b and 16b) (20% EtOAc/hexane), (c) (11S)-MIA-6,6′-dibromo-BINOLs (15c and 16c) (20% EtOAc/hexane), (d) (11S)-MIA-3,3′-dibromo-H$_8$-BINOLs (15d and 16d) (10% EtOAc/hexane), (e) (11S)-MIA-3,3′-dibromo-BINOLs (15e and 16e) (80% DCM/hexane), and (f) (11S)-MIA-BINAMs (15f and 16f) (10% EtOAc, 40% DCM/hexane).

were dried or distilled prior use following the standard procedures. Triethylamine was dried over CaH$_2$ and freshly distilled prior to use.

General procedure for synthesis of diastereomers of MIA-BINOL derivatives 15a–d

In the synthesis of (11S)-MIA-chiral-(R)-BINOL adducts 15a–d, (11S)-7 (168.9 mg, 0.524 mmol) was mixed with each chiral (R)-BINOL derivatives 9, 10, 11, or 13 (100 mg, 0.349 mmol) in anhydrous dichloromethane (DCM, 10 mL) in a 50 mL round-bottom flask equipped with a magnetic stir bar and a nitrogen gas inlet. Subsequently, DCC (108.1 mg, 0.524 mmol) and DMAP (6.4 mg, 0.052 mmol) were added as coupling reagents to the stirring reaction mixture at 0 °C. The reaction mixture was then allowed to warm to ambient temperature and

stirred for an additional 24 h. Upon completion, the reaction mixture was concentrated under reduced pressure, and the crude product was purified by PLC to afford the desired diastereomers.

(+)-(R,11S)-Carbo-[2″-hydroxy-(1′,1″-binaphthalen)-2′-oxy]-11-carbomethoxymethyl-9,10-dihydro-9,10-ethanoanthracene, 15a. Pale yellow solid (96.0 mg, 53%). Mp 136–137 °C. $[\alpha]_D^{26.0}$ +250.04 (c 0.10, CHCl$_3$). R_f (20% EtOAc/hexane) 0.69. ^{1}H NMR (500 MHz, CDCl$_3$): δ = 8.00 (d, J = 9.0 Hz, 1H), 7.99–7.91 (m, 3H), 7.49 (dt, J = 3.9, 8.1 Hz, 1H), 7.44 (d, J = 8.9 Hz, 1H), 7.41 (ddd, J = 1.2, 6.8, 8.1 Hz, 1H), 7.38–7.32 (m, 3H), 7.29 (ddd, J = 1.4, 6.8, 8.2 Hz, 1H), 7.18–7.10 (m, 3H), 7.09–6.99 (m, 3H), 6.96 (td, J = 1.4, 7.5 Hz, 1H), 6.92 (dd, J = 1.8, 6.9 Hz, 1H), 6.65 (dd, J = 1.4, 7.2 Hz, 1H), 5.25 (s, 1H), 4.13 (t, J = 2.7 Hz, 1H), 3.55 (s, 1H), 3.41 (s, 3H), 2.43 (dd, J = 2.9, 13.1 Hz, 1H), 2.39 (d, J =
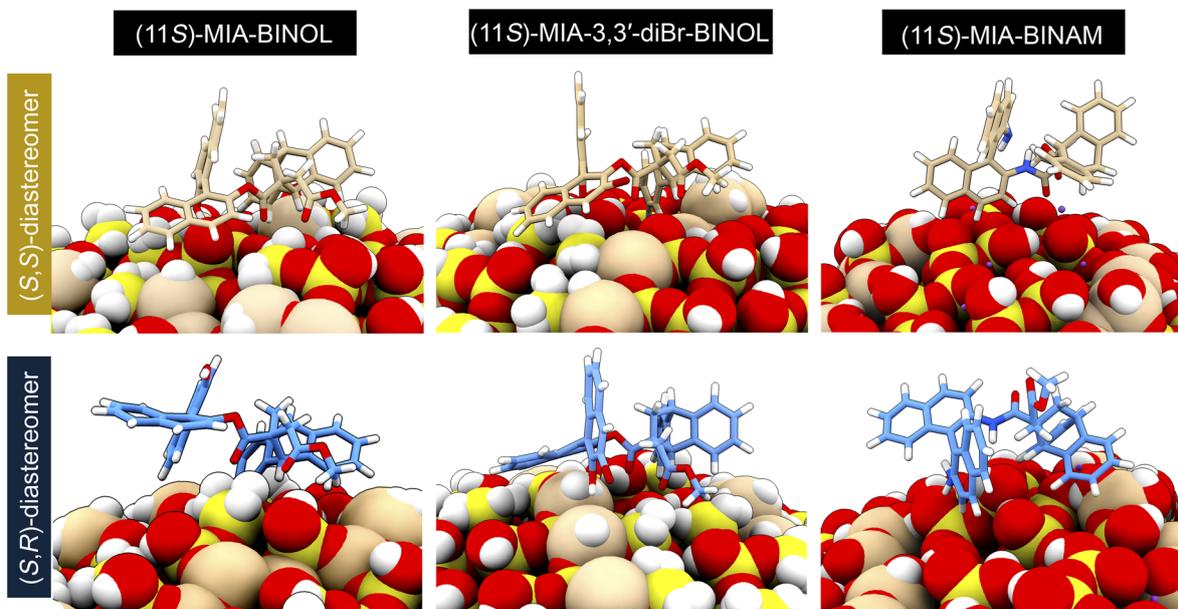

Fig. 9 3-Dimensional structures of adducts–silica gel complexes from the clustering of the simulation.

16.8 Hz, 1H), 1.68 (d, J = 16.8 Hz, 1H), 1.30 (dd, J = 2.7, 13.0 Hz, 1H). ^{13}C NMR (125 MHz, CDCl$_3$): δ = 172.5, 171.2, 151.7, 147.9, 143.1, 142.6, 139.6, 139.2, 133.7, 132.9, 131.9, 130.4, 130.4, 129.1, 128.3, 128.0, 127.4, 126.7, 126.6, 126.4, 126.1, 125.7, 125.7, 125.6, 125.5, 125.0, 124.8, 123.6, 123.4, 123.2, 121.3 (2), 118.3, 114.2, 52.0, 51.5, 49.9, 43.9, 43.8, 36.9. HRMS (ESI) calcd for C$_{40}$H$_{31}$O$_5$ [M + H]$^+$ m/z 591.2171 found 591.2174.

(+)-(R,11S)-Carbo-[2″-hydroxy-(1′,1″-bi(5′,5″,6′,6″,7′,7″,8′,8″-octahydronaphthalen))-2′-oxy]-11-carbomethoxymethyl-9,10-dihydro-9,10-ethanoanthracene, 15b. White solid (122.2 mg, 60%). Mp 122–123 °C. $[α]_D^{25.3}$ +110.02 (c 0.10, CHCl$_3$). R_f (20% EtOAc/hexane) 0.44. ^{1}H NMR (500 MHz, CDCl$_3$): δ = 7.26–7.21 (m, 2H), 7.17–6.99 (m, 8H), 6.90 (d, J = 8.4 Hz, 1H), 6.86 (d, J = 8.4 Hz, 1H), 4.82 (s, 1H), 4.25 (t, J = 2.7 Hz, 1H), 3.96 (s, 1H), 3.55 (s, 3H), 2.88–2.77 (m, 4H), 2.56 (d, J = 16.8 Hz, 1H), 2.50 (dd, J = 2.9, 13.1 Hz, 1H), 2.43 (dt, J = 6.1, 17.2 Hz, 1H), 2.30–2.15 (m, 2H), 2.05 (dt, J = 6.1, 17.1 Hz, 1H), 1.88 (d, J = 16.8 Hz, 1H), 1.85–1.65 (m, 8H), 1.47 (dd, J = 2.7, 13.1 Hz, 1H). ^{13}C NMR (125 MHz, CDCl$_3$): δ = 172.4, 171.2, 150.5, 146.7, 143.2, 142.8, 140.0, 139.5, 137.8, 136.1, 135.4, 130.1, 129.7, 129.3, 126.5, 126.4, 126.3, 125.8, 125.7, 125.4, 125.2, 123.4, 123.0, 122.1, 119.0, 113.4, 52.1, 51.5, 49.8, 43.9, 43.9, 37.2, 29.5, 29.4, 27.2, 26.8, 23.1 (2), 22.8, 22.6. HRMS (ESI) calcd for C$_{40}$H$_{39}$O$_5$ [M + H]$^+$ m/z 599.2797 found 599.2791.

(+)-(R,11S)-Carbo-[6′,6″-dibromoomo-2″-hydroxy-(1′,1″-bi-naphthalen)-2′-oxy]-11-carbomethoxymethyl-9,10-dihydro-9,10-ethanoanthracene, 15c. White solid (73.5 mg, 47%). Mp 132–133 °C. $[α]_D^{26.8}$ +130.02 (c 0.10, CHCl$_3$). R_f (20% EtOAc/hexane) 0.57. ^{1}H NMR (500 MHz, CDCl$_3$): δ = 8.14–7.97 (m, 2H), 7.95–7.79 (m, 2H), 7.44–7.36 (m, 2H), 7.33–7.26 (m, 2H), 7.21–7.14 (m, 1H), 7.14–7.00 (m, 6H), 6.96 (td, J = 1.3, 7.5 Hz, 1H), 6.85 (d, J = 9.0 Hz, 1H), 6.72 (dd, J = 1.2, 7.3 Hz, 1H), 5.27 (s, 1H), 4.11 (t, J = 2.7 Hz, 1H), 3.85 (s, 1H), 3.44 (s, 3H), 2.41 (d, J = 16.6 Hz, 1H), 2.28 (dd, J = 3.0, 13.2 Hz, 1H), 1.86 (d, J = 16.6 Hz, 1H), 1.30 (dd, J = 2.7, 13.2 Hz, 1H). ^{13}C NMR (125 MHz, CDCl$_3$): δ = 172.9, 171.1, 152.0, 148.2, 143.1, 142.7, 139.6, 139.3, 133.0, 132.1, 131.5, 130.8, 130.3, 130.1 (2), 130.0, 129.6 (2), 127.2, 126.7, 126.5 (2), 125.8, 125.6, 125.5, 124.8, 123.4, 123.3, 122.7, 121.6, 120.4, 119.5, 117.5, 113.9, 51.7, 51.6, 49.9, 43.9, 43.7, 37.2. HRMS (ESI) calcd for C$_{40}$H$_{29}$O$_5$Br$_2$ [M + H]$^+$ m/z 749.0356 found 749.0352.

(+)-(R,11S)-Carbo-[3′,3″-dibromoomo-2″-hydroxy-(1′,1″-bi(5′,5″,6′,6″,7′,7″,8′,8″-octahydronaphthalen))-2′-oxy]-11-carbomethoxymethyl-9,10-dihydro-9,10-ethanoanthracene, 15d. White solid (29.5 mg, 38%). Mp 144–145 °C. $[α]_D^{25.0}$ +140.02 (c 0.10, CHCl$_3$). R_f (10% EtOAc/hexane) 0.57. ^{1}H NMR (500 MHz, CDCl$_3$): δ = 7.43–7.38 (m, 1H), 7.30 (s, 1H), 7.25–7.20 (m, 2H), 7.18–7.13 (m, 2H), 7.11–7.00 (m, 4H), 5.27 (br s, 1H), 4.79 (s, 1H), 4.15 (t, J = 2.7 Hz, 1H), 3.59 (s, 3H), 2.76–2.65 (m, 4H), 2.32–2.10 (m, 2H), 2.06–1.75 (m, 6H), 1.75–1.55 (m, 8H). ^{13}C NMR (125 MHz, CDCl$_3$): δ = 171.9, 170.4, 147.2, 143.9, 143.6, 142.5, 140.9, 140.6, 137.5, 137.0, 136.0, 133.6, 132.3, 131.2, 130.1, 127.2, 126.4, 125.7 (2), 125.6, 125.3, 123.6, 123.3, 122.4, 113.2, 108.3, 51.5, 49.1, 49.0, 44.0, 42.8, 39.2, 29.3, 28.9, 26.6 (2), 22.6 (2), 22.5, 22.3. HRMS (ESI) calcd for C$_{40}$H$_{37}$O$_5$Br$_2$ [M + H]$^+$ m/z 757.0987 found 757.0958.

General procedure for synthesis of diastereomers of MIA-BINOL derivatives 16a–d

Analogous to the synthesis of 15a–d, the preparation of (11S)-MIA-chiral-(S)-BINOL adducts 16a–d was carried out by combining (11S)-7 (168.9 mg, 0.524 mmol) with each of the chiral (S)-BINOL derivatives 9, 10, 11, or 13 (100 mg, 0.349 mmol) in anhydrous dichloromethane (DCM, 10 mL) within a 50 mL round-bottom flask fitted with a magnetic stir bar and nitrogen inlet. DCC (108.1 mg, 0.524 mmol) and DMAP (6.4 mg, 0.052 mmol) were then introduced as coupling agents to the reaction mixture, which was maintained at 0 °C. The reaction was subsequently brought to room temperature and stirred for an additional 24 hours. After the reaction was complete, the solvent was removed under reduced pressure, and the resulting crude product was purified by PLC to yield the desired diastereomers.

(+)-(S,11S)-Carbo-[2″-hydroxy-(1′,1″-binaphthalen)-2′-oxy]-11-carbomethoxymethyl-9,10-dihydro-9,10-ethanoanthracene, 16a. White solid (102.3 mg, 56%). Mp 190–191 °C. $[α]_D^{25.1}$ +90.02 (c 0.10, CHCl$_3$). R_f (20% EtOAc/hexane) 0.58. ^{1}H NMR (500 MHz, CDCl$_3$): δ = 7.99 (d, J = 8.9 Hz, 1H), 7.97–7.88 (m, 3H), 7.48 (ddd, J = 1.4, 6.7, 8.2 Hz, 1H), 7.45 (d, J = 9.0 Hz, 1H), 7.41 (ddd, J = 1.2, 6.7, 8.1 Hz, 1H), 7.36–7.30 (m, 3H), 7.28 (dd, J = 1.2, 8.4 Hz, 1H), 7.20–7.15 (m, 2H), 7.12 (dd, J = 1.0, 8.5 Hz, 1H), 7.10–7.03 (m, 3H), 7.01 (td, J = 1.2, 7.5 Hz, 1H), 6.77 (td, J = 1.2, 7.5 Hz, 1H), 6.37 (dd, J = 1.1, 7.4 Hz, 1H), 5.12 (s, 1H), 4.15 (t, J = 2.7 Hz, 1H), 3.86 (s, 1H), 3.46 (s, 3H), 2.43 (dd, J = 3.0, 13.2 Hz, 1H), 2.31 (d, J = 16.5 Hz, 1H), 1.78 (d, J = 16.5 Hz, 1H), 1.33 (dd, J = 2.7, 13.1 Hz, 1H). ^{13}C NMR (125 MHz, CDCl$_3$): δ = 172.3, 171.0, 151.8, 147.9, 143.3, 142.6, 139.6, 139.3, 133.7, 133.3, 131.9, 130.4, 130.2, 129.0, 128.2, 128.1, 127.2, 126.8, 126.6, 126.4, 126.0, 125.8, 125.7, 125.6, 125.6, 125.0, 124.8, 123.5, 123.3 (2), 121.6, 121.3, 118.1, 113.9, 51.8, 51.6, 49.9, 43.8, 43.7, 36.9. HRMS (ESI) calcd for C$_{40}$H$_{31}$O$_5$ [M + H]$^+$ m/z 591.2171 found 591.2179.

(−)-(S,11S)-Carbo-[2″-hydroxy-(1′,1″-bi(5′,5″,6′,6″,7′,7″,8′,8″-octahydronaphthalen))-2′-oxy]-11-carbomethoxymethyl-9,10-dihydro-9,10-ethanoanthracene, 16b. White solid (126.8 mg, 62%). Mp 149–150 °C. $[α]_D^{25.5}$ −20.00 (c 0.10, CHCl$_3$). R_f (20% EtOAc/hexane) 0.34. ^{1}H NMR (500 MHz, CDCl$_3$): δ = 7.25–7.20 (m, 3H), 7.19–7.05 (m, 6H), 6.99 (d, J = 8.2 Hz, 1H), 6.94 (d, J = 8.4 Hz, 1H), 6.67 (d, J = 8.2 Hz, 1H), 4.57 (s, 1H), 4.32 (s, 1H), 4.20 (t, J = 2.7 Hz, 1H), 3.52 (s, 3H), 2.89–2.67 (m, 4H), 2.45–2.29 (m, 4H), 2.20–2.08 (m, 2H), 2.02 (d, J = 16.2 Hz, 1H), 1.87–1.63 (m, 8H), 1.44 (dd, J = 2.6, 13.1 Hz, 1H). ^{13}C NMR (125 MHz, CDCl$_3$): δ = 172.7, 170.6, 150.5, 146.8, 143.5, 142.9, 139.8 (2), 137.9, 135.5 (2), 130.0, 129.6, 129.1, 127.0, 126.5, 126.3, 125.7, 125.6, 125.5, 125.1, 123.5, 123.3, 122.0, 119.0, 113.8, 51.6, 51.5, 49.8, 43.9, 43.4, 36.8, 29.5, 29.3, 27.4, 26.8, 23.2 (2), 22.8, 22.6. HRMS (ESI) calcd for C$_{40}$H$_{39}$O$_5$ [M + H]$^+$ m/z 599.2797 found 599.2819.

(+)-(S,11S)-Carbo-[6′,6″-dibromoomo-2″-hydroxy-(1′,1″-bi-naphthalen)-2′-oxy]-11-carbomethoxymethyl-9,10-dihydro-9,10-ethanoanthracene, 16c. White solid (71.6 mg, 46%). Mp 137–139 °C. $[α]_D^{26.5}$ +24.00 (c 0.10, CHCl$_3$). R_f (20% EtOAc/hexane) 0.42. ^{1}H NMR (500 MHz, CDCl$_3$): δ = 8.18–7.99 (m, 2H), 7.90

(d, J = 9.0 Hz, 1H), 7.85 (d, J = 9.0 Hz, 1H), 7.45 (d, J = 9.0 Hz, 1H), 7.42–7.35 (m, 2H), 7.33 (d, J = 9.0 Hz, 1H), 7.23–7.15 (m, 2H), 7.15–6.99 (m, 5H), 6.91 (d, J = 9.0 Hz, 1H), 6.81 (td, J = 1.4, 7.5 Hz, 1H), 6.41 (d, J = 6.9 Hz, 1H), 5.23 (s, 1H), 4.17 (t, J = 2.7 Hz, 1H), 3.94 (s, 1H), 3.48 (s, 3H), 2.45–2.30 (m, 2H), 1.87 (d, J = 16.5 Hz, 1H), 1.35 (dd, J = 2.7, 13.1 Hz, 1H). ^{13}C NMR (125 MHz, CDCl$_3$): δ = 172.5, 170.9, 152.2, 148.1, 143.1, 142.7, 139.5, 139.2, 132.9, 132.1, 131.8, 130.7, 130.3, 130.1 (2), 130.0, 129.6, 129.4, 127.3, 126.7, 126.6, 126.4, 125.8, 125.6 (2), 124.7, 123.4, 123.3, 122.7, 121.8, 120.4, 119.5, 117.4, 113.8, 51.7, 51.6, 49.9, 43.8, 43.7, 37.2. HRMS (ESI) calcd for C$_{40}$H$_{29}$O$_5$Br$_2$ [M + H]$^+$ m/z 749.0356 found 749.0357.

(+)-(S,11S)-Carbo-[3′,3″-dibromoomo-2″-hydroxy-(1′,1″-bi(5-′,5″,6′,6″,7′,7″,8′,8″-octahydronaphthalen))-2′-oxy]-11-carbomethoxymethyl-9,10-dihydro-9,10-ethanoanthracene, 16d. White solid (29.1 mg, 37%). Mp 133–134 °C. $[\alpha]_D^{25.0}$ +40.01 (c 0.10, CHCl$_3$). R_f (10% EtOAc/hexane) 0.65. ^{1}H NMR (500 MHz, CDCl$_3$): δ = 7.39–7.32 (m, 1H), 7.32 (s, 1H), 7.21 (dd, J = 1.8, 7.0 Hz, 1H), 7.21–7.13 (m, 3H), 7.12–7.01 (m, 4H), 4.93 (s, 1H), 4.89 (br s, 1H), 4.11 (t, J = 2.7 Hz, 1H), 3.59 (s, 3H), 2.78–2.68 (m, 4H), 2.52–2.13 (m, 3H), 2.06–1.84 (m, 2H), 1.80–1.53 (m, 11H). ^{13}C NMR (125 MHz, CDCl$_3$): δ = 171.8, 170.4, 147.0, 143.5, 143.4, 142.5, 141.1, 140.5, 137.5, 137.0, 133.5, 131.2, 130.4, 126.8, 126.4, 125.8 (2), 125.2, 123.6, 123.3, 122.5, 113.0, 107.9, 51.4, 48.9, 48.6, 43.9, 42.7, 39.8, 29.3, 29.1, 26.8, 26.6, 22.7, 22.6, 22.5, 22.3. HRMS (ESI) calcd for C$_{40}$H$_{37}$O$_5$Br$_2$ [M + H]$^+$ m/z 757.0987 found 757.0980.

General procedure for synthesis of diastereomers of MIA-BINOL derivatives 15e–f

To a 50 mL round-bottom flask fitted with a magnetic stir bar and nitrogen inlet, a solution of (11S)-7 (170.0 mg, 0.0527 mmol) in DCM was added. At 0 °C, oxalyl chloride (0.06 mL, 0.703 mmol) was added, followed by a few drops of NEt$_3$ via needle-syringe. The solution was then stirred at ambient temperature for 4 hours under a nitrogen atmosphere. To remove residual oxalyl chloride, the reaction mixture was evaporated and further concentrated in vacuo. The resulting crude product was dissolved in DCM. Subsequently, a solution of enantiopure (R)-BINOL derivatives, 12 (for the synthesis of 15e) or BINAMs, 14 (for the synthesis of 15f) (100.0 mg, 0.352 mmol) in DCM, along with NEt$_3$ (0.01 mL, 0.703 mmol), was added under a nitrogen atmosphere at 0 °C. The reaction was stirred at room temperature for 24 hours. Upon completion, the crude solution was extracted three times with DCM/H$_2$O, followed by purification using PLC technique to obtain the desired diastereomers.

(+)-(R,11S)-Carbo-[3′,3″-dibromoomo-2″-hydroxy-(1′,1″-binaphthalen)-2′-oxy]-11-carbomethoxymethyl-9,10-dihydro-9,10-ethanoanthracene, 15e. White solid (36.1 mg, 42%). Mp 145–146 °C. $[\alpha]_D^{25.0}$ +130.46 (c 0.12, CHCl$_3$). R_f (80% DCM/hexane) 0.44. ^{1}H NMR (500 MHz, CDCl$_3$): δ = 8.21 (s, 1H), 8.17 (s, 1H), 7.81 (d, J = 8.1 Hz, 1H), 7.75 (d, J = 8.2 Hz, 1H), 7.47 (ddd, J = 1.2, 6.7, 8.2 Hz, 1H), 7.38–7.28 (m, 2H), 7.27–7.08 (m, 5H), 7.08–6.99 (m, 2H), 6.98–6.89 (m, 3H), 6.86 (d, J = 8.5 Hz, 1H), 5.76 (s, 1H), 4.67 (s, 1H), 4.02 (br t, 1H), 3.54 (s, 3H), 2.26–1.95 (br m, 1H), 1.92–1.74 (br m, 1H), 1.63–1.53 (m, 1H), 1.43 (dd, J = 3.0, 13.2 Hz, 1H). ^{13}C NMR (125 MHz, CDCl$_3$): δ = 170.1, 144.6, 143.4, 142.6, 140.5, 140.3, 133.4, 132.7, 132.5, 132.4, 132.0, 129.3, 127.5, 127.3, 127.2, 127.1, 126.9, 126.8, 126.4, 125.9, 125.7 (2), 125.5, 125.4, 124.9, 124.6, 123.5, 122.4, 115.6, 115.4, 51.5, 49.3, 48.7, 43.9, 42.6, 39.4. HRMS (ESI) calcd for C$_{40}$H$_{29}$O$_5$Br$_2$ [M + H]$^+$ m/z 749.0356 found 749.0318.

(+)-(R,11S)-Carbo-[2″-amine-(1′,1″-binaphthalen)-2′-amino]-11-carbomethoxymethyl-9,10-dihydro-9,10-ethanoanthracene, 15f. Brown solid (78.2 mg, 42%). Mp 120–121 °C. $[\alpha]_D^{30.4}$ −227.31 (c 0.11, toluene). R_f (10% EtOAc, 40% DCM/hexane) 0.31. ^{1}H NMR (500 MHz, toluene-d_8): δ = 8.86 (d, J = 9.2 Hz, 1H), 7.71–7.61 (m, 3H), 7.58 (d, J = 8.1 Hz, 1H), 7.19 (dd, J = 1.1, 8.5 Hz, 1H), 7.14–7.05 (m, 2H), 7.04–6.99 (m, 1H), 6.98–6.82 (m, 7H), 6.74 (d, J = 8.7 Hz, 1H), 6.69 (dd, J = 1.0, 8.4 Hz, 1H), 6.63 (td, J = 2.2, 7.2 Hz, 1H), 6.42–6.30 (m, 2H), 4.24 (s, 1H), 3.69 (t, J = 2.8 Hz, 1H), 3.35 (s, 2H), 3.11 (s, 3H), 2.84 (d, J = 16.8 Hz, 1H), 2.14–2.07 (m, 1H), 1.74 (d, J = 16.8 Hz, 1H), 1.46 (dd, J = 2.7, 14.3 Hz, 1H). ^{13}C NMR (125 MHz, toluene-d_8): δ = 172.3, 171.8, 143.8, 143.6, 142.0, 140.6, 140.4, 135.6, 134.5, 133.3, 131.6, 130.2, 129.2, 128.4, 128.3, 127.4, 126.8, 126.7, 126.6, 126.1, 125.9, 125.8, 125.7, 124.8, 123.3, 123.1, 122.6, 121.3, 121.0, 118.4, 110.8, 53.4, 51.6, 50.9, 44.8, 44.3, 39.0. HRMS (ESI) calcd for C$_{40}$H$_{33}$O$_3$N$_2$ [M + H]$^+$ m/z 589.2486 found 589.2494.

General procedure for synthesis of diastereomers of MIA-BINOL derivatives 16e–f

A solution of (11S)-7 (170.0 mg, 0.0527 mmol) in DCM was transferred to a 50 mL round-bottom flask equipped with a magnetic stir bar and a nitrogen inlet. Oxalyl chloride (0.06 mL, 0.703 mmol) was added at 0 °C, followed by the addition of a few drops of NEt$_3$ via needle-syringe. The mixture was stirred at ambient temperature for 4 hours under a nitrogen atmosphere. Following completion, the reaction mixture was evaporated and concentrated in vacuo to remove residual oxalyl chloride. The crude residue was then dissolved in DCM.

Next, a solution of enantiopure (S)-BINOL derivatives, 12 (for the synthesis of 16e) or BINAMs, 14 (for the synthesis of 16f) (100.0 mg, 0.352 mmol) in DCM, together with NEt$_3$ (0.01 mL, 0.703 mmol), was added at 0 °C under a nitrogen atmosphere. The reaction mixture was stirred at room temperature for 24 hours. Upon completion, the mixture was extracted three times with DCM/H$_2$O, and the combined organic extracts were purified by preparative layer chromatography (PLC) to afford the desired diastereomers.

(−)-(S,11S)-Carbo-[3′,3″-dibromoomo-2″-hydroxy-(1′,1″-binaphthalen)-2′-oxy]-11-carbomethoxymethyl-9,10-dihydro-9,10-ethanoanthracene, 16e. White solid (31.1 mg, 41%). Mp 168–170 °C. $[\alpha]_D^{25.0}$ −10.00 (c 0.10, CHCl$_3$). R_f (80% DCM/hexane) 0.57. ^{1}H NMR (500 MHz, CDCl$_3$): δ = 8.24 (s, 1H), 8.18 (s, 1H), 7.84–7.77 (m, 2H), 7.47 (ddd, J = 1.4, 3.9, 6.8, 8.2 Hz, 1H), 7.38 (ddd, J = 1.3, 6.9, 8.2 Hz, 1H), 7.33–7.25 (m, 2H), 7.20–6.75 (m, 10H), 5.59 (br s, 1H), 4.54 (s, 1H), 4.04 (br t, 1H), 3.32 (s, 3H), 2.20 (br d, J = 14.3 Hz, 1H), 1.93–1.73 (m, 2H), 1.44 (dd, J = 3.0, 13.2 Hz, 1H). ^{13}C NMR (125 MHz, CDCl$_3$): δ = 170.3, 144.4, 143.4, 142.5, 140.7, 140.2, 133.5, 132.7, 132.6, 132.1, 129.4,

127.5, 127.2, 127.1, 127.0, 126.5, 126.4, 126.1, 125.9, 125.8 (2), 125.7, 125.3, 124.6, 123.6, 122.6, 115.8, 115.3, 51.3, 49.1, 49.1, 43.9, 42.8, 39.5. HRMS (ESI) calcd for $C_{40}H_{29}O_5Br_2$ [M + H]$^+$ m/z 749.0356 found 749.0347.

(+)-(S,11S)-Carbo-[2″-amine-(1′,1″-binaphthalen)-2′-amino]-11-carbomethoxymethyl-9,10-dihydro-9,10-ethanoanthracene, 16f. Yellow solid (80.2 mg, 44%). Mp 142–143 °C. $[\alpha]_D^{24.5}$ +100.02 (c 0.09, toluene). R_f (10% EtOAc, 40% DCM/hexane) 0.42. ^{1}H NMR (500 MHz, toluene-d_8): δ = 8.77 (d, J = 9.0 Hz, 1H), 7.70–7.61 (m, 3H), 7.59 (d, J = 8.1 Hz, 1H), 7.44 (s, 1H), 7.29 (dd, J = 1.0, 8.5 Hz, 1H), 7.13 (ddd, J = 1.2, 6.7, 8.1 Hz, 1H), 7.07 (dd, J = 2.0, 5.8 Hz, 1H), 7.05–6.89 (m, 4H), 6.89–6.81 (m, 4H), 6.74 (td, J = 1.4, 7.3 Hz, 1H), 6.71 (d, J = 8.9 Hz, 1H), 6.63 (dd, J = 1.6, 7.4 Hz, 1H), 6.59 (td, J = 1.3, 7.4 Hz, 1H), 4.23 (s, 1H), 3.73 (t, J = 2.7 Hz, 1H), 3.09 (s, 3H), 2.98 (s, 2H), 2.36 (d, J = 16.2 Hz, 1H), 2.08–2.04 (m, 1H), 1.90 (d, J = 16.2 Hz, 1H), 1.31 (dd, J = 2.7, 13.6 Hz, 1H). ^{13}C NMR (125 MHz, toluene-d_8): δ = 172.1, 171.0, 143.6, 143.5, 143.4, 140.9, 140.6, 135.9, 134.5, 133.2, 131.8, 130.1, 129.2, 128.6, 128.5, 126.8, 126.6, 126.3, 126.1, 126.0, 125.8, 125.7 (2), 124.6, 123.5, 123.4, 122.8, 121.9, 121.4, 118.5, 111.1, 52.5, 51.6, 50.9, 45.0, 44.6, 38.3. HRMS (ESI) calcd for $C_{40}H_{33}O_3N_2$ [M + H]$^+$ m/z 589.2486 found 589.2467.

In accordance with previous publications,[19–21] the synthesis of (11R)-**8** was successfully accomplished. To broaden the application of these adducts as chiral resolving agents, (11R)-MIA-BINOL derivatives were also prepared. The physical properties and spectroscopic data for these compounds are provided in the SI. Furthermore, their capabilities in resolving racemic BINOL derivatives were investigated using TLC.

Computational methods

DFT calculations. The structures were established by using Chem3D software and exported as mol2 format. The structure was then energy minimization by using Amber10:EHT forcefield. The possible conformer was then searched by using "conformation search" module as implemented in Molecular Operating Environment (MOE) version 2015. The dihedral angle between the binapthyl ring of BINOLs was restrained in the ranges of 60 to 120°. The LowModeMD method was employed as the search algorithm with the rejection limit and iteration limit of 100 and 10 000 steps, respectively. The RMS gradient and RMSD limit were defined as 0.005 and 0.25 Å, respectively. All possible conformers were then undergone geometrical optimization by using DFT calculations at B3LYP level with 6-31G (d,p) as basis set using Gaussian16 package. The optimized structures were then ranked by the single point energy. The top 10 conformers were then optimized by using M06-2X/6-311++G (d,p) level of theory. Frequency calculation was applied for ensuring the structure to be at a local minimum structure. Finally, the lowest energy conformer was selected for visualization.

Molecular dynamics simulations. The silica gel was modeled based on the structure of α-cristobalite using the online tool CHARMM-GUI web interface as available on https://www.charmm-gui.org/ with the sphere radius of 30 Å resulting in 167,872.4 Å of material volume using INTERFACE force field. The ionization of surface was defined as 13.3 percent corresponding to the standard protonation state at pH 7. The structures of compounds and solvent molecules were prepared using Gaussview6 software followed by geometrical optimization using DFT at B3LYP/6-31G (d,p) as basis set for calculation on Gaussian16 package. The ligand topology was performed using the online tool SWISSPARAM as available on https://www.swissparam.ch/ based on the CHARMM22 force field. The compound was placed far from the silica gel surface with a distance of 10 Å.

All molecular dynamics simulations were carried out using GROMACS 2022 package on HPE apollo 6500 Gen10 on AMD EPYC 7742 CPUs with NVIDIA HGX A100 GPU. The complex was placed on cubic box and solvated by mix solvent between dichloromethane and hexane in the ratio of 50 %v/v with the distance between the surface of Si and the edge of the box of 20 Å. The system undergone energy minimization using steepest descent (SD) algorithm with the energy tolerance of 10 kJ mol^{-1} nm^{-1} followed by the conjugate gradient (CG) algorithm. The system was equilibrated in NVT ensemble followed by NPT ensemble performed for 500 ps per each. The long-range electrostatic interaction was calculated based on the Particle Mesh Ewald (PME) method with the cut-off value of 12 Å. The van der Waals interaction was calculated based on the cut-off method with the cut-off value of 12 Å. The covalent bonds between the hydrogen and heavy atoms were constrained using the LINear Constraint Solver (LINCS) algorithm. The Berendsen thermostat and Parrinello–Rahman barostat were used for temperature and pressure coupling, respectively. The time step was defined as 2 femtosecond and the trajectory was captured in every 5 ps. All complexes were performed in three independent replica copies with the distinct random seed values for atomic initial velocity generation. The molecular dynamics of each MIA-BINOL complex was performed for 100 ns at the temperature of 298 K and 1 atmospheric pressure.

The dynamics of the complex was determined using root-mean-square deviation (RMSD) as calculated by using gmx_rms command. The hydrogen bond was monitored using gmx_hbond module with the cut-off value of 3.5 Å. The distance between compound and silica gel surface was measured using $gmx\_mindist$ command. The visualization of molecular dynamics results was conducted using VMD version 1.9.4 package. The graph plotting was achieved on our in-house Python script.

Conclusion

We successfully synthesized diastereomers of MIAs and BINOL derivatives in good yields under mild conditions. The presence of bromine atoms at the 3 and 3′ positions of BINOLs led to distinct patterns in both the H_y proton behaviour in ^{1}H NMR and TLC resolution. DFT calculations revealed that the differing H_y proton behaviour is linked to the orientation of the second naphthol ring. The distinct TLC resolution, on the other hand, is attributed to significant differences in the number of hydrogen bonds formed between each diastereomer and the silica substrate, as optimized by MD simulations. Furthermore, stereochemical trends can be preliminarily inferred from TLC analysis. When (11S)-MIA is used as the chiral resolving agent (CRA), a higher R_f value is indicative of the (R)-configuration in

BINOL derivatives lacking 3,3′-dibromo substituents, and of the (S)-configuration in 3,3′-dibromo-substituted BINOLs and BI-NAMs. Conversely, a lower R_f value suggests the opposite enantiomeric configuration.

Author contributions

Wichai Sinthopweha: investigation, methodology, validation, formal analysis and writing – original draft. Nopawit Khamto: investigation, methodology, data curation, formal analysis and writing – original draft. Puracheth Rithchumpon: conceptualization, validation, supervision and writing – review & editing. Puttinan Meepowpan: conceptualization, writing – review & editing, resources and project administration.

Conflicts of interest

There are no conflicts to declare.

Data availability

The datasets used and/or analysed during the current study are available from the corresponding author on reasonable request.

CCDC 2344320, 2344660, 2423443 and 2423445 contain the supplementary crystallographic data for this paper.[23–26]

The supplementary information provides synthetic procedures, full characterization data (^{1}H NMR, ^{13}C NMR, HRMS) for compounds **17a–f** and **18a–f**, single-crystal X-ray diffraction information, and computational details. See DOI: https://doi.org/10.1039/d5ra04790k.

Notes and references

1 Y. B. Wang and B. Tan, *Acc. Chem. Res.*, 2018, **51**, 534–547.
2 R. Noyori, I. Tomino, Y. Tanimoto and M. Nishizawa, *J. Am. Chem. Soc.*, 1984, **106**, 6709–6716.
3 S. Kobayashi and H. Ishitani, *J. Am. Chem. Soc.*, 1994, **116**, 4083–4084.
4 J. M. Brune, *Chem. Rev.*, 2007, **107**, PR1–PR45.
5 M. McCarthy and P. J. Guiry, *Tetrahedron*, 2001, **57**, 3809–3844.
6 K. Takaishi, S. Murakami, F. Yoshinami and T. Ema, *Angew. Chem., Int. Ed.*, 2022, **61**, e202204609.
7 Y. Imai, K. Kamon, T. Kinuta, N. Tajima, T. Sato, R. Kuroda and Y. Matsubara, *Tetrahedron*, 2007, **63**, 11928–11932.
8 B. Paul, C. Näther, K. M. Fromm and C. Janiak, *CrystEngComm*, 2005, **7**, 309–319.
9 S. Narute, R. Parnes, F. D. Toste and D. Pappo, *J. Am. Chem. Soc.*, 2016, **138**, 16553–16560.
10 F. Wongso, H. Hidajata and A. K. Ray, *Sep. Purif. Technol.*, 2005, **46**, 168–191.
11 B. M. Panchal, C. Einhorn and J. Einhorn, *Tetrahedron Lett.*, 2002, **43**, 9245–9248.
12 M. Del Bubba, L. Checchini and L. Lepri, *Anal. Bioanal. Chem.*, 2013, **405**, 533–554.
13 R. Santos, K. V. Pontes and I. B. R. Nogueira, *Encyclopedia*, 2022, **2**, 151–188.
14 Z. Shan, F. Cheng, S. Huang, D. Zhao and Z. Jing, *Tetrahedron: Asymmetry*, 1997, **8**, 1175–1177.
15 J. X. Cai, Z. H. Zhou, K. Y. Li, C. H. Yeung and C. C. Tang, *Phosphorus, Sulfur Silicon Relat. Elem.*, 2002, **177**, 189–193.
16 K. Kodama, F. Takasea and T. Hirose, *RSC Adv.*, 2021, **11**, 18162–18170.
17 H. F. Chow, C. W. Wan and M. K. Ng, *J. Org. Chem.*, 1996, **61**, 8712–8714.
18 K. Dolsophon, N. Ruangsupapichat, J. Soponpong, S. Sunsuwan, S. Prabpai, P. Kongsaeree and T. Thongpanchang, *Tetrahedron: Asymmetry*, 2016, **27**, 1113–1120.
19 N. Intakaew, P. Rithchumpon, C. Prommin, S. Yimklan, N. Kungwan, P. Thavornyutikarn and P. Meepowpan, *Org. Biomol. Chem.*, 2019, **17**, 541–554.
20 P. Rithchumpon, N. Intakaew, N. Khamto, S. Yimklan, P. Nimmanpipug, P. Thavornyutikarn and P. Meepowpan, *Org. Biomol. Chem.*, 2021, **19**, 8955–8967.
21 P. Rithchumpon, N. Khamto, C. Kongsak, W. Saema, S. Duangdesh, V. Choommongkol and P. Meepowpan, *Tetrahedron*, 2023, **143**, 133545.
22 P. Labute, *J. Chem. Inf. Model.*, 2010, **50**, 792–800.
23 W. Sinthopweha, N. Khamto, P. Rithchumpon and P. Meepowpan, CCDC 2344320: Experimental Crystal Structure Determination, 2025, DOI: 10.5517/ccdc.csd.cc2jpg7y.
24 W. Sinthopweha, N. Khamto, P. Rithchumpon and P. Meepowpan, CCDC 2344660: Experimental Crystal Structure Determination, 2025, DOI: 10.5517/ccdc.csd.cc2jpt68.
25 W. Sinthopweha, N. Khamto, P. Rithchumpon and P. Meepowpan, CCDC 2423443: Experimental Crystal Structure Determination, 2025, DOI: 10.5517/ccdc.csd.cc2mbslc.
26 W. Sinthopweha, N. Khamto, P. Rithchumpon and P. Meepowpan, CCDC 2423445: Experimental Crystal Structure Determination5, 2025, DOI: 10.5517/ccdc.csd.cc2mbsnf.